Applied Physics Letters

Nanospectroscopy of a single patch antenna strongly coupled to a mid-infrared intersubband transition in a quantum well

Cite as: Appl. Phys. Lett. **117**, 101104 (2020); https://doi.org/10.1063/5.0018865
Submitted: 18 June 2020 . Accepted: 24 August 2020 . Published Online: 10 September 2020

Raymond Gillibert, Mario Malerba, Davide Spirito, Valeria Giliberti, Lianhe Li, A. Giles Davies, Edmund H. Linfield, Leonetta Baldassarre, Raffaele Colombelli, and Michele Ortolani

Applied Physics Letters ARTICLE scitation.org/journal/apl

Nanospectroscopy of a single patch antenna strongly coupled to a mid-infrared intersubband transition in a quantum well

Cite as: Appl. Phys. Lett. **117**, 101104 (2020); doi: 10.1063/5.0018865
Submitted: 18 June 2020 · Accepted: 24 August 2020 ·
Published Online: 10 September 2020

View Online Export Citation CrossMark

Raymond Gillibert,[1,a)] Mario Malerba,[2,b)] Davide Spirito,[3] Valeria Giliberti,[4] Lianhe Li,[5] A. Giles Davies,[5] Edmund H. Linfield,[5] Leonetta Baldassarre,[1,3] Raffaele Colombelli,[2] and Michele Ortolani[1,4,c)]

AFFILIATIONS

[1]Department of Physics, Sapienza University of Rome, 00185 Rome, Italy
[2]Centre de Nanosciences et de Nanotechnologies (C2N), CNRS UMR 9001, Université Paris-Saclay, 91120 Palaiseau, France
[3]IHP–Leibniz-Institut für Innovative Mikroelektronik, Im Technologiepark 25, D-15236 Frankfurt (Oder), Germany
[4]Center for Life Nanoscience, Istituto Italiano di Tecnologia (IIT), 00169 Rome, Italy
[5]School of Electronic and Electrical Engineering, University of Leeds, Woodhouse Lane, Leeds LS2 9JT, United Kingdom

[a)]E-mail: raymond.gillibert@roma1.infn.it
[b)]E-mail: mario.malerba@u-psud.fr
[c)]Author to whom correspondence should be addressed: michele.ortolani@roma1.infn.it

ABSTRACT

Scanning-probe-assisted mid-infrared nano-spectroscopy is employed to reveal the polaritonic dispersion of individual MIM (metal-insulator-metal) square patch antennas whose modes can be strongly coupled to a mid-infrared intersubband transition. The patch antenna side length L sets the resonances between $\lambda = 5.5\ \mu$m and $12.5\ \mu$m. The active region consists of a highly doped AlInAs/InGaAs/AlInAs single quantum well that presents an intersubband transition at $1190\ \mathrm{cm}^{-1}$ ($\lambda = 8.4\ \mu$m). When the patch antenna optical resonance approaches and matches the intersubband transition frequency ($L \sim 1.8\ \mu$m), a clear anticrossing behavior—evidence of strong coupling—is observed in the near-field scattering phase spectra of individual antennas. The measured Rabi splitting is 4.5 THz. The near-field scattering spectra agree with the far-field extinction spectra acquired on arrays of identical antennas.

Intersubband (ISB) transitions in semiconductor quantum wells (QWs) enable the implementation of devices operating in the mid-IR (and THz) spectral ranges, such as the quantum cascade laser[1] and the quantum well infrared photodetector.[2] Furthermore, they are important in the study of fundamental physical phenomena at very long wavelengths, such as non-linearities, cavity electrodynamics (CED), and strong light-matter coupling. In the latter regime, when the light-matter coupling is stronger than the dephasing mechanisms in the system, new quasi-particles—called ISB polaritons—emerge.[3,4] ISB polaritons have been subject to much theoretical and experimental work since their first observation, with developments including ISB polariton LEDs,[5,6] polariton-based detectors,[7] ultra-fast switching,[8] and ultra-strongly coupled systems.[9,10]

Recently, the study of ISB polaritons at the single resonator level has started to attract interest. This partly stems from experience in the visible and near-infrared spectral ranges, where it is possible to operate on isolated resonators with very high Q/V values (Q is the quality factor and V is the resonator *modal* volume).[11] This has been, however, challenging in the mid-IR and THz spectral ranges because the detectors are less efficient, among other factors. With standard far-field techniques, only ensembles of a few cavities can be measured.[12,13] Remarkably, using thermal fluctuations as an internal source of electromagnetic field, a single patch cavity could be studied,[14] but a temperature of 433 K was necessary, which is possibly not compatible with strong light-matter coupling.

Operating in the electromagnetic near-field offers an alternative way to access the optical properties of a single resonator at very long wavelengths. Near-field scattering optical microscopy (SNOM) techniques, based on scanning probes approaching the object, have recently been exploited to study empty cavities[15] and systems operating in the weak coupling regime.[16–19] The challenge when moving to the strong-coupling regime is to maintain an elevated electromagnetic overlap with the active region—to obtain a large Rabi splitting—while permitting a non-negligible fraction of the electric field to leak outside the cavity in the form of "fringing" fields that can be scattered by the scanning probe.

In mid-IR/THz polaritonics, metallic cavities, typically in a metal-insulator-metal (MIM) architecture, are almost exclusively used, with the *patch antenna* proving the most effective in terms of electromagnetic confinement, tailorable radiative coupling,[20,21] and easy implementation in more complex devices. Its extreme confinement properties explain why there is no report of near-field field spectroscopy on patch antennas strongly coupled to ISB transitions in QWs, although an initial demonstration has been very recently given in *dogbone* antennas coupled to ISB transitions.[19]

In this Letter, we show that judicious design and careful experimentation permit broadband SNOM nanospectroscopy to be performed on a single patch antenna strongly coupled to a mid-IR ISB transition: the polaritonic resonances appear in the near-field scattering phase spectra of single antenna cavities, indicating that strong coupling is achieved in individual resonators and antenna arrays are not required.

In our MIM antenna, the two mirrors of the optical cavity are formed by a top gold patch (square of side L) and a bottom gold backplane. The cavity contains a dielectric layer (polymer, inserted for the purpose of photothermal expansion imaging, see below) and a heterostructure semiconductor (a heavily n-doped multisubband QW). The electromagnetic simulations, performed with an FDTD (finite-differences time-domain) approach [Fig. 1(a)], reveal a strong field confinement in the cavity, as expected, with small fringing field regions that will be employed for SNOM spectroscopy of each single resonator of side L.

The final realization of a typical sample is represented in Figs. 1(b) and 1(c). The two-level system is constituted by a single highly doped

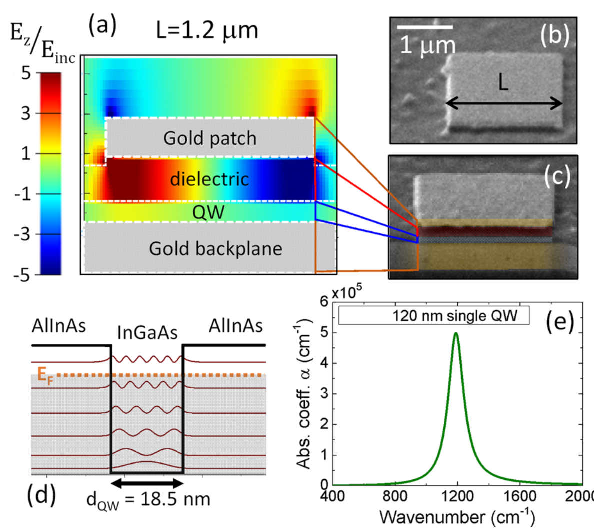

FIG. 1. (a) Simulated pattern of the vertical component of the electric field enhancement (E_z/E_{inc}) in a patch antenna with its cavity filled with a 200 nm-thick dielectric layer and a 120 nm-thick semiconductor layer containing a QW. (b) SEM image of a single patch antenna of length $L = 2.3\,\mu$m and (c) FIB cross section of another antenna with layers highlighted in color. (d) QW structure leading to an intersubband (ISB) transition at 1190 cm^{-1}, whose absorption spectrum is shown in (e).

($n = 10^{19}\,e^-/cm^3$) QW [AlInAs 25 nm/InGaAs 18.5 nm/AlInAs 25 nm, Fig. 1(d)], exhibiting a multisubband ISB transition in the mid-IR at 1190 cm^{-1} [$E_2 - E_1 = 148$ meV, Fig. 1(e)]. In the fabrication process, the active region was coated with a metallic layer (10 nm Ti/100 nm Au, e-beam evaporated) and subsequently bonded to a clean GaAs host wafer with a commercial epoxy adhesive (Epo-tek 353-ND, Epoxy Technology). The pristine InP growth substrate was then removed in HCl, exposing the InGaAs etch-stop layer (40 nm) above the QW structure. A 200 nm-thick polymeric layer (polymerized EPON 812 by Sigma Aldrich) was cut with an ultramicrotome (Leica EM UC7) and transferred – exploiting the high surface tension of distilled water, which keeps the thin epitaxial layer unfolded and stretched – onto the semiconductor active region.[22] A 100 nm-thick gold layer was finally evaporated on top of the resist. The final step was the implementation of patch antennas in layouts of either arrays (between 100 and 150 elements, depending on the value of L; periodicity in arrays P = 2L) or of single isolated cavities, using focused ion beam patterning to etch away the unwanted gold. A few tens of nanometers of polymer were etched and removed as well, without, however, affecting the optical response. The arrays were used to measure far-field extinction spectra using unpolarized light with a Fourier transform IR spectroscopy (FT-IR) micro-reflectance setup in the 600–4000 cm^{-1} range (Nicolet Continuum), equipped with a 32×, 0.65 NA Cassegrain objective.

As stated previously, access to a scattering-type SNOM of the patch antenna cavity, where the field is confined, is a problem. Near-field imaging of the mode profile cannot be performed by scanning the patch antenna surface, as the field is practically zero above the top metallization [Fig. 1(a)]. To access the field distribution in an alternative way, we, thus, explored photothermal expansion microscopy to obtain a sub-diffraction-limit-resolved image of the patch antenna cavity. In this technique, a monochromatic IR laser beam is focused on a scanning probe (similar to SNOM), but instead of the scattered radiation, the mechanical atomic force microscopy (AFM) signal is acquired. The local thermal expansion is measured by opto-mechanical analysis of the AFM cantilever oscillations at the repetition rate of the IR laser (AFM-IR technique).[23–25] In our case, radiation energy absorption is sensed at a specific xy position inside the antenna cavity by determining the IR-induced thermal expansion at that position, with the probe tip scanning the surface of the gold patch. In order to enhance this AFM-IR signal and the imaging resolution, a 200 nm-thick layer of EPON 812 polymer (that features a high thermal expansion coefficient and a poor lateral thermal conductivity) is inserted into the antenna cavity during sample fabrication. The AFM-IR measurements were performed using a NanoIR2 (Anasys Instruments), using the same configuration employed in SNOM measurements: a gold-coated probe tip, 70° incidence of the IR laser beam, and the radiation electric field linearly polarized in the incidence plane (p-polarization).

The spectra of the IR radiation scattered by single antennas were collected with a SNOM microscope (NeaSNOM from NeaSpec). Linearly polarized broadband IR radiation, obtained from difference-frequency generation, is focused on the gold-coated AFM probe tip, operating in the tapping mode, through a parabolic mirror that is also used to collect the backscattered radiation. The detected signal is amplitude-modulated at the mechanical tapping frequency ~220 kHz. Because of the non-linear dependence of the near-field interaction from the tip-to-sample distance, at higher harmonics n (with $n \geq 2$), the near-field signal from the tip-antenna interaction is dominant over the linear far-field background. The scattering spectra are extracted using the nano-FTIR technique in which the tip and the sample are in an arm of a Michelson interferometer, thereby providing both the amplitude and phase of the backscattered radiation.[26] The spectra were taken with the probe tip located at the bottom right antenna corner on which the light impinges first, where the highest signal intensity was observed [see Fig. 2(c), X mark]. The measurements were taken by averaging 10 interferograms with a spectral resolution of 8 cm^{-1}.[27] The demodulated phase and amplitude signals are normalized to the reference quantities measured on an Au film deposited far from the antennas,

$$\eta_n(\omega) = s_n^{norm}\, e^{i\phi_n^{norm}} = \frac{s_n^{antenna}}{s_n^{ref}}\, e^{i\left(\phi_n^{antenna}-\phi_n^{ref}\right)}, \tag{1}$$

where s is the near-field amplitude, ϕ is the phase, and the suffix n indicates the nth harmonic demodulation used to suppress the far-field background. In the case of absorbing materials, in the limit of sample thickness larger than the inverse characteristic value of the in-plane momentum excited by the probe tip,[28] it has been shown that the far-field absorption peak positions correspond to those in the imaginary part of the SNOM signal: $\mathrm{Im}(\eta_n) = s_n^{norm} \sin\phi_n^{norm}$. For thinner samples, the peak position in the scattering phase (ϕ_n^{norm}) or in $\mathrm{Im}(\eta)$ corresponds to features typically observed in grazing-incidence IR reflection spectroscopy with p-polarized light.[27,29] For complex structures such as antennas, the scattering coefficient will be the result of the electromagnetic interaction of the tip with the antenna (in our case, also coupled to the QW transition) and with the substrate. This interaction can be described either as coupled harmonic oscillators[17] or as a set of complex optical impedances.[27] As a result, the SNOM observations of complex tip-antenna systems strongly vary in the literature depending on the relative interaction strength of the antenna and the tip with the exciting radiation and the relative delay of this interaction, resulting in a dip in the SNOM signal amplitude, a dispersive step-like behavior in the phase,[4] a peak in the imaginary part, or a step-like feature in the imaginary part.[17]

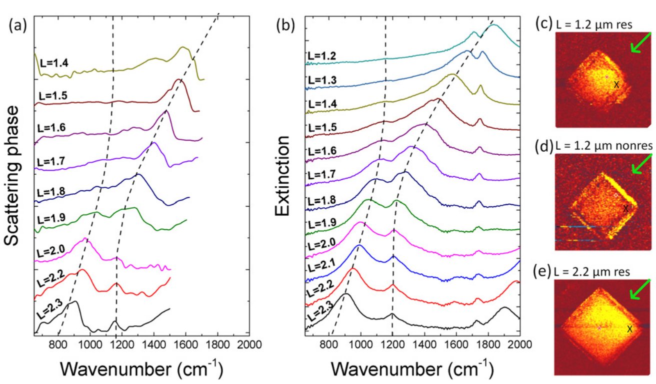

FIG. 2. (a) SNOM scattering for most of the cavities. The dashed lines are guides to the eye. (b) FTIR extinction (defined as the sum of absorption and scattering) for all the cavities using unpolarized light. L-values are reported on the left side. (c)–(e) AFM-IR maps for L = 1.2 μm at 1830 cm^{-1} excitation [(c) antenna resonance] and at 950 cm^{-1} [(d) non-resonant wavenumber] and for L = 2.2 μm at 950 cm^{-1} [(e) antenna resonance]. The green arrow indicates the direction of the incoming IR beam, and the cross indicates the location at which the SNOM signal was collected.

Experimentally, we observed peaks in ϕ^{norm} [Fig. 2(a)] as well as in $\mathrm{Im}(\eta)$ (not shown). The peaks in $\mathrm{Im}(\eta)$ are always red-shifted, within the width-at-half-maximum of the ϕ^{norm} peak for all L, and so analyzing $\mathrm{Im}(\eta)$ instead of ϕ^{norm} would not impact the following discussion.

The near-field scattering spectra in Fig. 2(a) exhibit a clear anti-crossing behavior, with a minimum splitting obtained for $L = 1.9\,\mu$m. In this case, the full width at half maximum for both polaritons is found to be 195 cm^{-1}. This value is approximately equal to the splitting energy (205 cm^{-1}) and indicates a strong-coupling regime,[30] further corroborated by comparison with the extinction measurements performed in the far-field with a FTIR microscope on patch antenna arrays [Fig. 2(b)]. The range of L-values where the strong coupling is observed, and the polariton peak positions and their relative peak intensity, as measured with the two techniques (near-field vs far-field), are similar. However, for $L < 1.5\,\mu$m, where the detuning is large and only one uncoupled-antenna peak is observed, the near-field (SNOM) peak is slightly blue-shifted when compared to the far-field (FTIR) peak.[31,32] The polariton dispersion is highlighted by the same lines that are guides to the eye in both Figs. 2(a) and 2(b) (dashed black curves). The data in Fig. 2(a) are a clear indication of strong coupling to ISB transitions in isolated individual antenna resonators, such as the patch antenna in Fig. 1(c). A peak located at 1738 cm^{-1}, corresponding to the C = O stretching vibration in the EPON polymer, is visible in the FTIR spectra [Fig. 2(b)] and couples also with the plasmon resonance of the patch antenna for L = 1.3–1.2 μm, leading to an asymmetric resonance and a surface-enhanced infrared absorption (SEIRA) effect.

In Fig. 2(a), with $L = 2.2\,\mu$m and $L = 2.3\,\mu$m, the shoulder of a high frequency peak can be seen (not fully shown in the graph for clarity). This peak is attributed to the second-order antenna resonance, which couples very strongly to the probe. The AFM-IR maps in Figs. 2(c)–2(e), taken far from strong coupling for clarity ($L = 2.2\,\mu$m and $L = 1.2\,\mu$m), show that a single antenna can be correctly excited by a gold-coated AFM probe when the wavelength is resonant with the antenna mode, the incidence angle is 70°, and the radiation electric-field polarization is TM (p-polarized wave), like in the SNOM experiment.

In Fig. 3, we summarize the SNOM nanospectroscopy results (red stars) and compare them to far-field spectroscopy (blue dots). Both series of data points have been obtained by fitting of the spectra in Fig. 2 with Lorentzian functions that reproduce the main spectral features. The analytical prediction for strong coupling based on the secular equation is shown as a continuous green line,[12] which are the roots of the following *secular equation* that is an implicit equation for ω:

$$\left(\omega^2-\omega_{patch}^2\right)\left(\omega^2-\tilde{\omega}_{ISB}^2\right)=\Gamma_{opt}\, f_w\, \omega_{patch}^2\, \omega_{plasma}^2.$$

These roots correspond to the frequencies of upper and lower and polaritons,[10] ω_{patch} is the frequency of the patch antenna resonance (numerically calculated), $\tilde{\omega}_{ISB}$ is the experimental ISB frequency measured in a multi-pass waveguide configuration (it includes, therefore, the plasma polarization shift and, hence, the *tilde* sign), Γ_{opt} is the electromagnetic overlap factor with the active region, f_w is the ratio

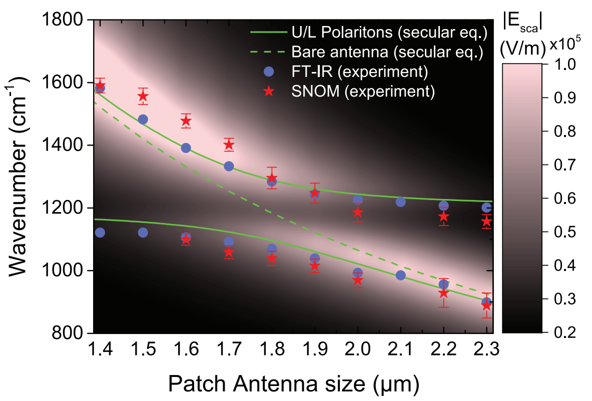

FIG. 3. Upper and lower polariton peak positions as detected by FTIR reflectivity measurements (blue dots), SNOM scattered peak position (red stars), and comparison with the analytical calculations in the case of strong coupling (green line) or for no coupling (dashed green line). The map plot of the simulated scattering field norm ($|E_{sca}|$) is superimposed and numerically calculated as the average electric field in a cubic region of 100^3 nm^3.

between the QW width and the semiconductor active region thickness, and ω_{plasma} is the ISB plasma frequency (obtained from the sample doping). The curve was fitted to the far-field data by adjusting Γ_{opt}. Strong coupling theory clearly explains both far-field and near-field spectra, at odds with a zero-coupling simulation of the antenna resonance frequency vs L shown as a dashed green line.

Substantial agreement between far-field and near-field spectroscopy data is observed, with the possible exception of the upper polariton branch for $L < 1.7\ \mu m$, where the near-field peaks are blue-shifted compared to the far-field data and to the theory. This is confirmed by numerical simulations (Comsol) of the local electric field intensity, calculated along the patch side on which the radiation impinges (map in the background). The EPON resist refractive index was adjusted to $n = 1.87$ to fit the observed Rabi splitting energy. We also verified that this combination would lead to the same overlap factor for the secular equation. The simulation can be taken as an estimate of the near-field scattering efficiency measured in SNOM and is also blue-shifted compared to the green curve and blue dots in the upper polariton branch for $L < 1.7\ \mu$m. Further studies are required to understand the small discrepancy observed between near-field and far-field resonances, but the general picture emerging from this work confirms that near-field observation of strong light-matter coupling in individual resonators yields consistent results. The SNOM spectra taken on single antennas show that there is no key difference in far-field and near-field analysis of strong-coupling systems and, therefore, that near-field spectroscopy analysis of single resonators with small resonator modal volume V is possible. For example, near-field spectroscopy probes could be used in future photonic integrated chips that would contain single resonators but certainly not entire arrays.

In conclusion, we have realized a series of patch-antenna cavities with varying resonance frequencies in the mid-infrared. The cavities contain a doped QW, whose optical transition is strongly coupled—despite the presence of a relatively thick layer of absorbing dielectric material—to the antenna resonance for specific values of the patch size. We have studied the far-field extinction spectra of arrays and the near-field scattering spectra of single antennas. Both sets of spectra revealed the two polariton branches emerging from operation in the strong light-matter coupling regime. Numerical simulations and analytical model predictions for strong coupling were verified in both experiments, indicating that strong-coupling features are intrinsic to single antenna cavities of subwavelength dimensions. The results are relevant for future nanoscale quantum devices exploiting patch cavities, such as non-linear meta-surfaces or efficient, fast-response mid-infrared detectors.

We thank D. Mailly and G. Patriarche for useful discussions and P. Filloux for cleanroom help. We acknowledge financial support from the European Union FET-Open Grant MIRBOSE (737017) and from the French National Research Agency (Project "IRENA," No. ANR-17-CE24-0016). We acknowledge the EPSRC program "HyperTerahertz" (No. EP/P021859/1). E.H.L. acknowledges support of the Royal Society and Wolfson Foundation. M.M. acknowledges the European Union's Horizon 2020 Research and Innovation Program, under the Marie Skłodowska Curie Grant Agreement No. 748071. This work was partly supported by the French RENATECH network. R.G., M.O., and L.B. acknowledge support from the Italian Ministry of Research through Program PRIN 2017, Grant No. 2017Z8TS5B. D.S. acknowledges the funding from the German Research Foundation (DFG) within the project ESSENCE. L. B. acknowledges support through the IHP Microelectronics "Wolfgang Mehr" Fellowship Award.

DATA AVAILABILITY

Meaningful data are provided in the text and the rest are available upon request by any reviewer.

REFERENCES

[1] Y. Yao, A. J. Hoffman, and C. F. Gmachl, Nat. Photonics **6**, 432 (2012).
[2] E. R. Weber, R. K. Willardson, H. C. Liu, and F. Capasso, *Intersubband Transitions in Quantum Wells: Physics and Device Applications* (Academic Press, 1999).
[3] C. Weisbuch, M. Nishioka, A. Ishikawa, and Y. Arakawa, Phys. Rev. Lett. **69**, 3314 (1992).
[4] D. Dini, R. Köhler, A. Tredicucci, G. Biasiol, and L. Sorba, Phys. Rev. Lett. **90**, 116401 (2003).
[5] L. Sapienza, A. Vasanelli, R. Colombelli, C. Ciuti, Y. Chassagneux, C. Manquest, U. Gennser, and C. Sirtori, Phys. Rev. Lett. **100**, 136806 (2008).
[6] M. Geiser, G. Scalari, F. Castellano, M. Beck, and J. Faist, Appl. Phys. Lett. **101**, 141118 (2012).
[7] P.-B. Vigneron, S. Pirotta, I. Carusotto, N.-L. Tran, G. Biasiol, J.-M. Manceau, A. Bousseksou, and R. Colombelli, Appl. Phys. Lett. **114**, 131104 (2019).
[8] G. Günter, A. A. Anappara, J. Hees, A. Sell, G. Biasiol, L. Sorba, S. De Liberato, C. Ciuti, A. Tredicucci, A. Leitenstorfer, and R. Huber, Nature **458**, 178 (2009).
[9] G. Scalari, C. Maissen, D. Turčinková, D. Hagenmüller, S. D. Liberato, C. Ciuti, C. Reichl, D. Schuh, W. Wegscheider, M. Beck, and J. Faist, Science **335**, 1323 (2012).
[10] Y. Todorov, A. M. Andrews, R. Colombelli, S. De Liberato, C. Ciuti, P. Klang, G. Strasser, and C. Sirtori, Phys. Rev. Lett. **105**, 196402 (2010).
[11] B. Deveaud, *The Physics of Semiconductor Microcavities* (John Wiley & Sons, 2007).
[12] M. Malerba, T. Ongarello, B. Paulillo, J.-M. Manceau, G. Beaudoin, I. Sagnes, F. De Angelis, and R. Colombelli, Appl. Phys. Lett. **109**, 021111 (2016).
[13] V. Giannini, Y. Francescato, H. Amrania, C. C. Phillips, and S. A. Maier, Nano Lett. **11**, 2835 (2011).
[14] C. Li, V. Krachmalnicoff, P. Bouchon, J. Jaeck, N. Bardou, R. Haïdar, and Y. De Wilde, Phys. Rev. Lett. **121**, 243901 (2018).
[15] O. Mitrofanov, Y. Todorov, D. Gacemi, A. Mottaghizadeh, C. Sirtori, I. Brener, and J. L. Reno, Opt. Express **26**, 7437 (2018).

[16]M. Schnell, A. García-Etxarri, A. J. Huber, K. Crozier, J. Aizpurua, and R. Hillenbrand, Nat. Photonics **3**, 287 (2009).
[17]E. A. Muller, B. Pollard, H. A. Bechtel, R. Adato, D. Etezadi, H. Altug, and M. B. Raschke, ACS Photonics **5**, 3594 (2018).
[18]A. García-Etxarri, I. Romero, F. J. García de Abajo, R. Hillenbrand, and J. Aizpurua, Phys. Rev. B **79**, 125439 (2009).
[19]C.-F. Wang, T. G. Habteyes, T. S. Luk, J. F. Klem, I. Brener, H.-T. Chen, and O. Mitrofanov, Nano Lett. **19**, 4620 (2019).
[20]Y. Todorov, L. Tosetto, J. Teissier, A. M. Andrews, P. Klang, R. Colombelli, I. Sagnes, G. Strasser, and C. Sirtori, Opt. Expres **18**, 13886 (2010).
[21]C. A. Balanis, *Antenna Theory: Analysis and Design* (John Wiley & Sons, 2016).
[22]N.-L. Tran, M. Malerba, A. Talneau, G. Biasiol, O. Ouznali, A. Bousseksou, J.-M. Manceau, and R. Colombelli, Opt. Express **27**, 1672 (2019).
[23]A. Dazzi and C. B. Prater, Chem. Rev. **117**, 5146 (2017).
[24]F. Lu, M. Jin, and M. A. Belkin, Nat. Photonics **8**, 307 (2014).
[25]V. Giliberti, L. Baldassarre, A. Rosa, V. de Turris, M. Ortolani, P. Calvani, and A. Nucara, Nanoscale **8**, 17560 (2016).
[26]F. Huth, A. Govyadinov, S. Amarie, W. Nuansing, F. Keilmann, and R. Hillenbrand, Nano Lett. **12**, 3973 (2012).
[27]S. Mastel, A. A. Govyadinov, T. V. A. G. de Oliveira, I. Amenabar, and R. Hillenbrand, Appl. Phys. Lett. **106**, 023113 (2015).
[28]L. M. Zhang, G. O. Andreev, Z. Fei, A. S. McLeod, G. Dominguez, M. Thiemens, A. H. Castro-Neto, D. N. Basov, and M. M. Fogler, Phys. Rev. B **85**, 075419 (2012).
[29]A. A. Govyadinov, I. Amenabar, F. Huth, P. S. Carney, and R. Hillenbrand, J. Phys. Chem. Lett. **4**, 1526 (2013).
[30]L. Novotny, Am. J. Phys. **78**, 1199 (2010).
[31]P. Alonso-González, P. Albella, F. Neubrech, C. Huck, J. Chen, F. Golmar, F. Casanova, L. E. Hueso, A. Pucci, J. Aizpurua, and R. Hillenbrand, Phys. Rev. Lett. **110**, 203902 (2013).
[32]B. M. Ross and L. P. Lee, Opt. Lett. **34**, 896 (2009).